Journal of Magnetism and Magnetic Materials 582 (2023) 170985

Contents lists available at ScienceDirect

Journal of Magnetism and Magnetic Materials

journal homepage: www.elsevier.com/locate/jmmm

Study of neodymium addition on the magnetic and structural properties of strontium hexaferrite synthesized by the Pechini method

M.F. Ramírez-Ayala [a], A. Lobo Guerrero [a,*], A.M. Herrera-González [a], T.J. Pérez-Juache [b], R. López-Juárez [b], J.T. Elizalde-Galindo [c], V.E. Salazar-Muñoz [d], S.A. Palomares-Sánchez [e], S.Y. Reyes-López [f]

[a] Área Académica de Ciencias de la Tierra y Materiales, Universidad Autónoma del Estado de Hidalgo, Carr. Pachuca-Tulancingo Km. 4.5, 42184 Hidalgo, México
[b] Unidad Morelia del Instituto de Investigaciones en Materiales, Universidad Nacional Autónoma de México, Antigua Carr. Pátzcuaro No. 8701, Col. Exhacienda de San José de La Huerta, C.P. 58190 Morelia, México
[c] Instituto de Ingeniería y Tecnología, Universidad Autónoma de Ciudad Juárez, Av. del Charro No. 450 Norte, C.P. 32310 Ciudad Juárez, México
[d] Facultad de Ingeniería, Universidad Autónoma de San Luis Potosí, Av. Manuel Nava 8, 78290 San Luis Potosí, México
[e] Facultad de Ciencias, Universidad Autónoma de San Luis Potosí, Av. Manuel Nava 8, C.P. 78290 San Luis Potosí, México
[f] Instituto de Ciencias Biomédicas, Universidad Autónoma de Ciudad Juárez, Envolvente del PRONAF y Estocolmo s/n, C.P. 32310 Ciudad Juárez, Chihuahua, México

ARTICLE INFO

Keywords:
Neodymium-doped
Strontium hexaferrite
Rietveld method
Rare earth
Pechini method

ABSTRACT

This work reports a systematic study of the effect of neodymium (Nd) on the microstructural, magnetic, and structural properties of strontium hexaferrite ($SrFe_{12}O_{19}$). Neodymium was incorporated during the hexaferrite fabrication using the sol–gel Pechini method. The results show that neodymium is partially incorporated into the hexaferrite crystal structure, allowing the formation of neodymium orthoferrite as a second phase, which dramatically affects the magnetic properties of the hexaferrite. The temperature in the range of 900 to 1100 °C and the variation of the neodymium content were two analytical variables that allowed to study the effects of neodymium on the hexaferrite properties. The behavior of the phases and their structural properties were investigated using X-ray diffraction and the Rietveld refinement method. The magnetic properties were obtained using vibrant sample magnetometry, and the microstructural characteristics were analyzed by electron microscopy. For the hexaferrite containing up to 2.85 wt% of neodymium orthoferrite, the maximum energy product (BH_{max}) was 35% higher than the one showed by the neodymium-free hexaferrite. The increased magnetic properties have been associated with the incorporation of neodymium in the hexaferrite structure and due to the magnetic interactions between the hexaferrite and neodymium orthoferrite.

1. Introduction

The strontium hexaferrite belongs to a family of iron-oxide synthetic compounds first developed in the 50s in the Philips laboratories. The use of these compounds has been widely expanded mainly due to their suitable physical properties and simple and cheap production processes. In recent years, hexaferrites have attracted much attention due to their excellent chemical stability, high Néel temperature, high corrosion resistance, and uniaxial magnetocrystalline anisotropy [1,2]. They find important applications as permanent magnets due to their relatively good energy product and the best performance-to-cost ratio [3,4]. However, that is not its only interesting functional property. Hexaferrites also have been used in electromagnetic interference shielding [5], high-frequency antenna [6], water treatment [7], hyperthermia [8], high-resistivity [9], and optical applications [10].

Strontium hexaferrite is a magnetic ceramic obtained from oxide powders at high sintering temperatures. This compound has a hexagonal symmetry, $P6_3/mmc$ space group and it is formed by a close-packed oxygen anions network where one Sr^{2+} cation replaces one of the O^{2-} anions. There are 24 iron cations distributed over five interstitial sublattices: 12 k, 2a, $4f_2$ (octahedral), $4f_1$ (tetrahedral), and 2b (bipyramidal). The high magnetocrystalline anisotropy exhibited by hexaferrites makes their crystal structure a key parameter that can significantly change their magnetic properties. In addition, the crystalline structure strongly depends on hexaferrite's chemical composition. Then, doping or substituting different cations of the hexaferrite with

* Corresponding author.
E-mail address: azdrubal.guerrero@cimav.edu.mx (A.L. Guerrero).

https://doi.org/10.1016/j.jmmm.2023.170985
Received 27 April 2023; Received in revised form 25 June 2023; Accepted 29 June 2023
Available online 5 July 2023

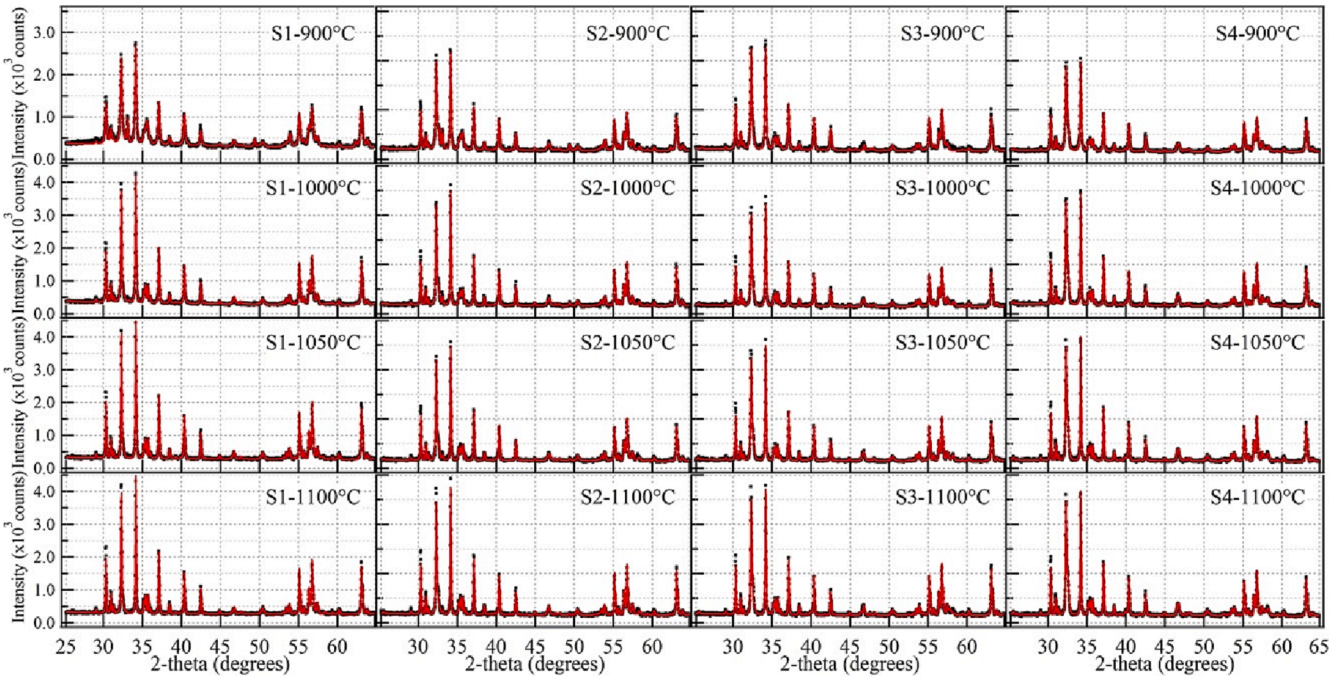

Fig. 1. X-ray diffraction patterns and Rietveld adjusts of the strontium hexaferrite substituted with neodymium and sintered at different temperatures.

other elements has important consequences on its electronic structure, superexchange lengths, and magnetocrystalline anisotropy energies [11–14].

Scientific interest in understanding the effect of different rare earths in the hexagonal ferrites has been revitalized [15–20]. Despite some interesting properties conferred on hexaferrites, the effects of neodymium are poorly understood [21–26]. Neodymium also appears to behave differently as the methods and fabrication parameters change [27,28]. The morphological characteristics and physical properties of the hexaferrite obtained by any method depend on several variables such as precursor ratio, sintering time, temperature, etc. The solid-state reaction method is one of the most used due to its simplicity, low production cost, and the possibility of obtaining micro-sized particles [29]. This method, although useful, has an important drawback since the high sintering temperature and the large particle size affect the hard-magnetic properties and could limit the use of hexaferrites in advanced applications. The chemical routes present a good alternative to obtain hexaferrite at low temperatures with controlled particle size and other microstructural characteristics [30–33]. The sol–gel Pechini method is a chemical method that offers simplicity, low-temperature synthesis, and low fabrication cost. This method provides good control of the microstructural characteristics i.e. shape anisotropy and uniform crystallite size, which is desirable for controlling the magnetic properties of the hexaferrite [34–36]. Previous work showed that hexaferrite prepared by the Pechini method at low calcination temperature strongly enhanced the magnetic properties in comparison with those hexaferrites prepared by different routes [37,38]. Also, it has been reported that the solubility of the rare earth in the hexaferrite depends on its own nature; for example, the praseodymium (Pr) showed a higher solubility than neodymium (Nd) [39,40]. In this work, we investigated the feasibility of using the sol–gel Pechini method to fabricate the substituted strontium hexaferrite, and the effects of the neodymium on the structure, microstructure, and magnetic properties.

2. Experimental

2.1. Synthesis

The sol–gel Pechini method requires the preparation of a polymeric resin from organic acids to obtain a desirable three-dimensional polymeric network [41,42]. Strontium nitrate $Sr(NO_3)_2$ (99 %, Sigma-Aldrich), iron nitrate $Fe(NO_3)_3{\cdot}9H_2O$ (99 %, Sigma-Aldrich), neodymium nitrate $Nd(NO_3)_3{\cdot}6H_2O$ (99 %, Sigma-Aldrich), citric acid monohydrate $C_6H_8O_7{\cdot}H_2O$ (99 %, JT Baker) and ethylene glycol $C_2H_6O_2$ (99 %, Sigma-Aldrich) were used for the hexaferrite preparation. The content of neodymium in the strontium hexaferrite was varied according to the formula $Sr_{1-x}Nd_xFe_{12}O_{19}$, whit $\times$ = 0.1, 0.2, 0.3, and 0.4. These samples were labeled as S1, S2, S3, and S4, respectively. The hexaferrite was obtained by dissolving stoichiometric amounts of metal nitrates following the chemical described in Equation (1), the citric acid was mixed in deionized water in a molar ratio of 5:1.

$$1-xSr(NO_3)_2+12Fe(NO_3)_3\bullet 9H_2O+xNd(NO_3)_3\bullet 6H_2O+C_6H_8O_7 \bullet H_2O+C_2H_6O_2\rightarrow Sr_{1-x}Nd_xFe_{12}O_{19}+CO_2\uparrow+NO_2\uparrow \quad (1)$$

The resultant solution was heated at 70 °C for dehydration and later further heated at 100 °C for polymerization. The obtained resin was precalcined at 370 °C for 45 min and grounded in an agate mortar and pestle. Finally, the powders were calcined at 900 °C, 1000 °C, 1050 °C and 1100 °C for 2 h, and cooled slowly in the air.

2.2. Characterization

The structural properties were analyzed using a D2 Phaser diffractometer (Bruker) with Cu Kα radiation ($K_{\alpha 1}$ = 1.5406 Å) within a 2θ angular range from 20° to 70°, with step size and step time of 0.02° and 0.6 s, respectively. The software Match! (Phase Analysis using Powder Diffraction) [43] was used to identify the presence of secondary phases. The Rietveld refinement method incorporated in the MAUD program [44] was used to evaluate the structural properties and to perform quantitative phase analysis. The structural model used for the refinement was based on the strontium hexaferrite: hexagonal symmetry with $P6_3/mmc$ space group and lattice parameters a = 5.884 Å, c = 23.05 Å

Table 1
Results of the Rietveld analysis for the strontium hexaferrite varying the neodymium content and the sintering temperature.

Sample	Lattice parameters		Density (g/cm^3)	Crystallite size (nm)	χ^2
	a (Å)	c (Å)			
$SrFe_{12}O_{19}$ (1050 °C)	5.8821 (4)	23.0518 (10)	5.105	86 (2)	1.321
S1-900 °C	5.8884 (2)	23.0780 (12)	5.088	81 (5)	1.385
S1-1000 °C	5.8864 (1)	23.0742 (5)	5.092	288 (4)	1.343
S1-1050 °C	5.8859 (1)	23.0713 (4)	5.094	832 (25)	1.404
S1-1100 °C	5.8860 (3)	23.0702 (4)	5.093	1009 (3)	1.448
S2-900 °C	5.8863 (2)	23.0735 (10)	5.093	121 (4)	1.290
S2-1000 °C	5.8854 (1)	23.0709 (4)	5.095	358 (22)	1.323
S2-1050 °C	5.8844 (2)	23.0680 (5)	5.097	958 (71)	1.264
S2-1100 °C	5.8844 (1)	23.0681 (5)	5.097	1079 (87)	1.461
S3-900 °C	5.8867 (1)	23.0657 (8)	5.094	137 (2)	1.281
S3-1000 °C	5.8861 (1)	23.0679 (6)	5.094	364 (11)	1.260
S3-1050 °C	5.8858 (1)	23.0696 (5)	5.094	690 (39)	1.303
S3-1100 °C	5.8853 (1)	23.0705 (5)	5.095	1062 (18)	1.505
S4-900 °C	5.8849 (1)	23.0644 (7)	5.097	160 (2)	1.189
S4-1000 °C	5.8850 (1)	23.0672 (5)	5.096	404 (13)	1.224
S4-1050 °C	5.8851 (1)	23.0733 (5)	5.095	1122 (84)	1.312
S4-1100 °C	5.8851 (1)	23.0733 (5)	5.094	1075 (89)	1.311

(COD ID: 1006000) [45]. Hematite (Fe_2O_3), trigonal, *R-3c*:R space group, lattice parameters a = 5.43 Å, α = 55.28° (COD ID: 1011240), and neodymium orthoferrite ($NdFeO_3$), orthorhombic, *Pnma* space group, lattice parameters a = 5.588 Å, b = 7.762 Å, c = 5.449 Å (COD ID: 2003124) also were considered. The morphological characteristics were studied using a scanning electron microscope (SEM) JEOL JSM-IT300, and transmission electron microscope (TEM) JEOL JEM-ARM200F. The magnetic properties were evaluated from the magnetization curves obtained at room temperature with a maximum applied field of 20 kOe, using a Quantum Design MPMS3 vibrating sample magnetometer (VSM).

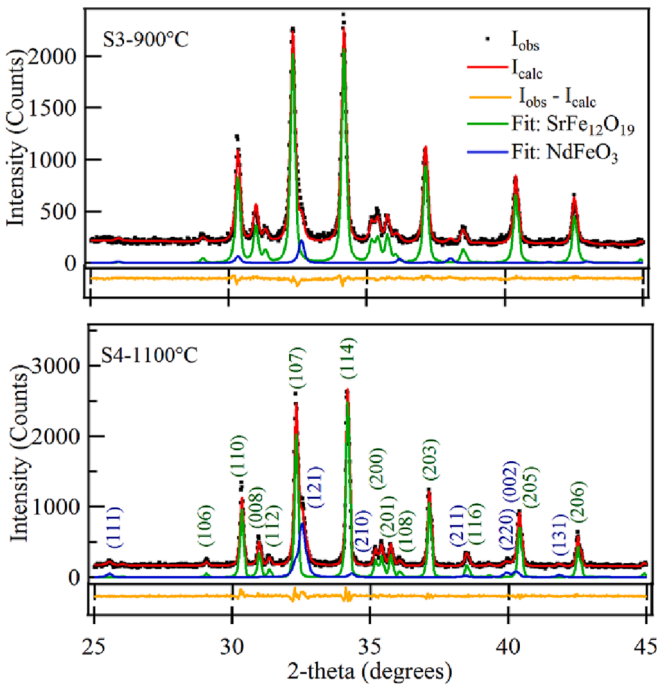

Fig. 3. X-ray patterns and the Rietveld fit of the samples S3-900 °C and the S4-1100 °C. The 2-theta range from 25 to 45° was selected for a better view. (Miller indices are indicated for each phase).

3. Results and discussion

3.1. Structural analysis

Fig. 1 shows the experimental X-ray diffraction patterns (dotted black lines) and the Rietveld fit (continuous red lines) for the strontium hexaferrite with increasing neodymium content and sintered at 900, 1000, 1050, and 1100 °C. Both the sintering temperature and neodymium content are responsible for the purity, crystallinity, and structural properties of hexaferrite. The lattice parameters, density, and

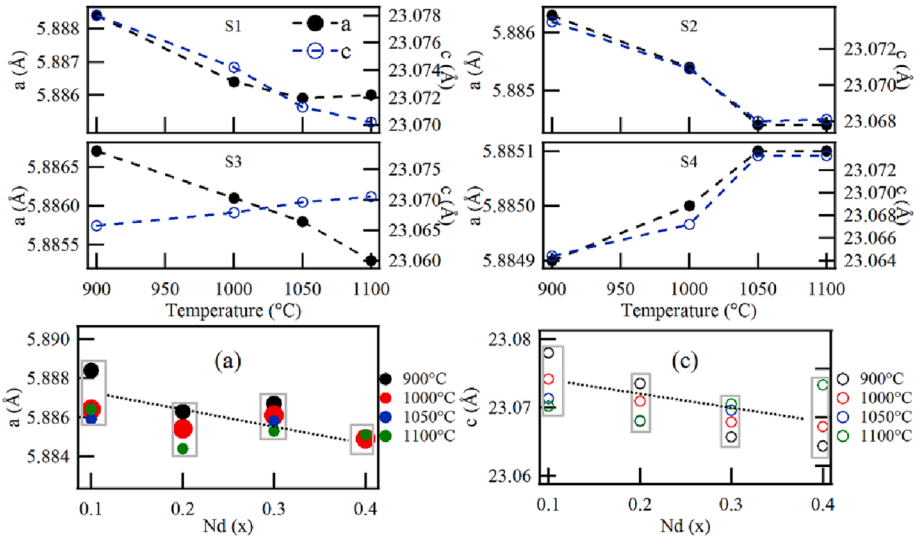

Fig. 2. Behavior of the hexaferrite lattice parameters *a*, and *c*, with respect to an increment of the sintering temperature and the neodymium content.

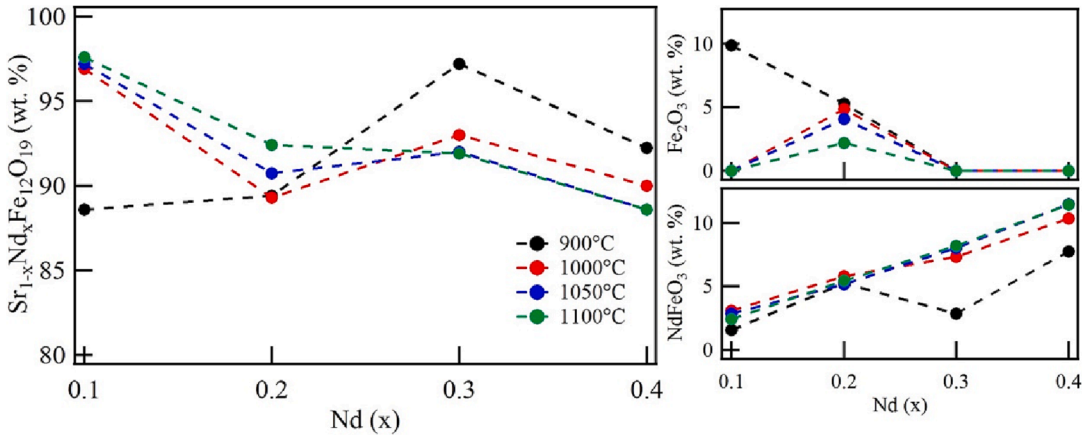

Fig. 4. Phase analysis of the samples varying the sintering temperature and the amount of neodymium content.

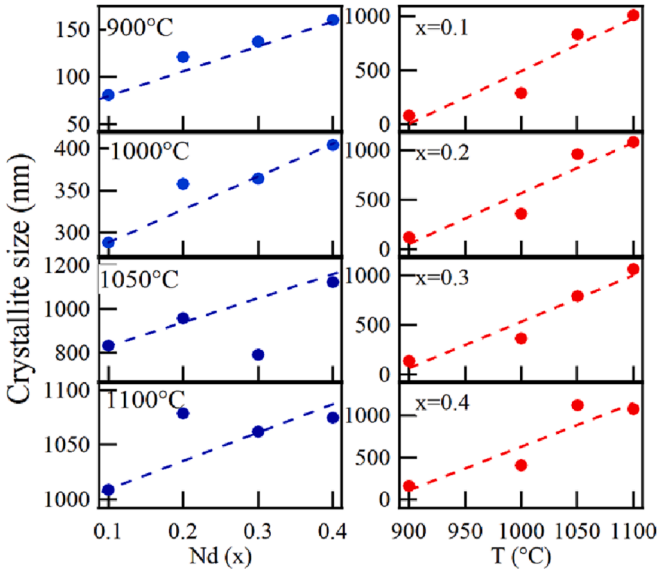

Fig. 5. Crystallite size behavior as a function of the neodymium content (left) and sintering temperature (right). (Dashed lines are guides for the eye).

crystallite size were obtained from the Rietveld refinement method and displayed in Table 1. The crystallite size was evaluated using the anisotropic size-strain broadening following the procedure indicated by Lutterotti et al. [44]. The structural parameters of the pure strontium hexaferrite obtained at 1050 °C were included for comparison purposes. The Chi-squared $\chi^2 = (R_{wp}/R_{exp})^2$ was provided for each sample because values between 1 and 2 ensure a good Rietveld refinement fit [46].

The lattice parameters obtained from the Rietveld analysis are shown in Fig. 2. Here, the *a* and *c* parameters of the S1 and S2 samples decrease as the calcination temperature increases. However, the lattice parameters suffer a slight increment as the temperature increases in samples S3 and S4 (when the neodymium content increases). Therefore, the change in the hexaferrite lattice parameters suggests that a limited amount of neodymium is incorporated into the hexaferrite structure. These results agree with previous works using other preparation methods showing that neodymium has low solubility in the strontium hexaferrite [47–49].

3.2. Phase analysis

Fig. 3 shows two X-ray diffraction patterns and the corresponding Rietveld fit for two samples with different amounts of neodymium orthoferrite (S3-900 °C) and (S4-1100 °C). This figure shows that it is difficult to see the presence of neodymium orthoferrite because its XRD peak overlaps with the main peak of hexaferrite with a slight distortion at the bottom of the peak. This characteristic can go unnoticed for small amounts of neodymium orthoferrite if a careful phase analysis is not carried out.

Fig. 4 shows the results of the phase analysis obtained from the studied samples. The strontium hexaferrite is difficult to form at 900 °C due to an incomplete chemical reaction that forms hematite as the second phase. However, increasing the amount of neodymium also increases the amount of hexaferrite formed at 900 °C. On the other hand, a higher quantity of the hexaferrite phase was observed with increasing sintering temperature. Although when high content of neodymium is used, the formation of neodymium orthoferrite is promoted, diminishing the amount of obtained hexaferrite. The Pechini sol–gel method allows limited neodymium solubility in the hexaferrite structure and favors neodymium orthoferrite formation where the neodymium excess does not incorporate into the magnetoplumbite structure.

3.3. Crystallite size

Fig. 5 shows the behavior of the crystallite size of the hexaferrite as a function of the neodymium content (left) and as a function of the sintering temperature (right). The crystallite size has a trend toward increasing as the neodymium amount and the sintering temperature increase. The smallest crystallite size was 81 nm obtained for $\times = 0.1$ at 900 °C (S1-900 °C). This nanosized crystallite size was expected due to the low calcination temperature. However, at this temperature, the crystallite size shows an increment at higher neodymium contents. The samples sintered at 1000, 1050, and 1100 °C show a similar behavior indicating that neodymium promotes the crystal growth in the hexaferrite. Thus, the small size of crystallites can be attained when low sintering temperatures and low neodymium contents are used. Besides, the crystal growth rate can be changed by changing the fabrication conditions. However, it also depends on the stress and strain of the structure due to changes in the lattice parameters, as the stress is absorbed by the defects, leading to changes in the crystallite growth kinetics [50].

3.4. Microstructural characterization

Fig. 6 shows the SEM micrographs of the hexaferrite particles calcined at different temperatures from 900 °C to 1100 °C, for $\times = 0.1$. The particles grow in the preferential growth direction and form elongated particles. The average particle size along the preferential growth direction increases from ~ 100 nm to ~ 1000 nm when the sintering temperature goes from 900 to 1100 °C. This behavior agrees with the results of crystallite size obtained from the Rietveld analysis.

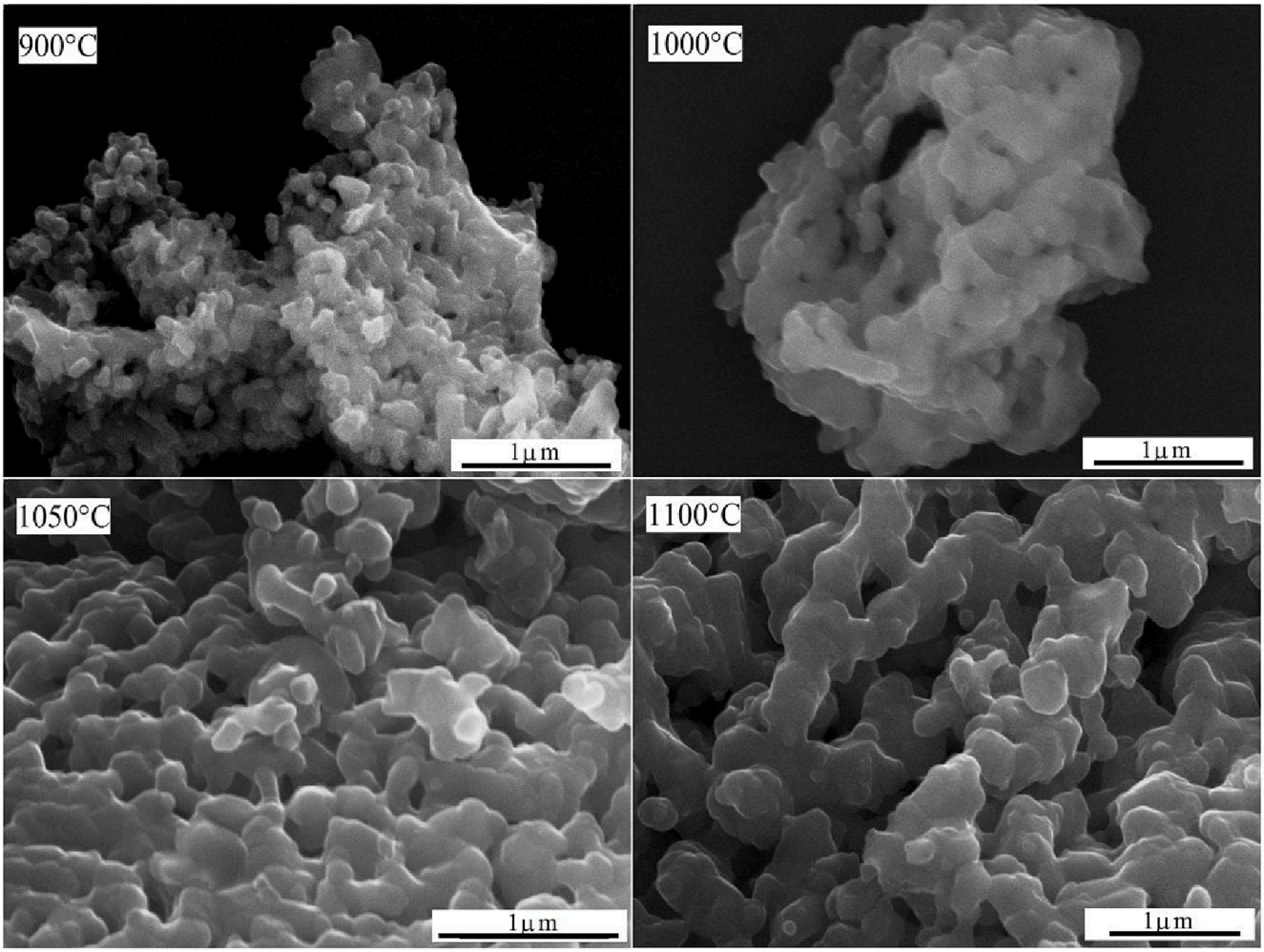

Fig. 6. SEM micrographs of the substituted hexaferrite sample with $\times$ = 0.1 at various sintering temperatures.

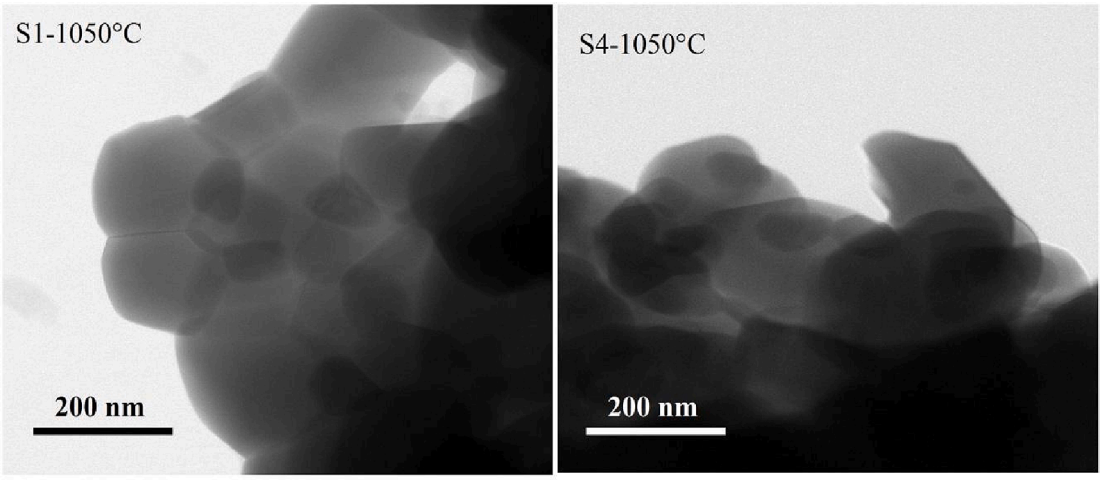

Fig. 7. TEM micrographs obtained from the samples sintering at 1050 °C with the lower and higher neodymium contents.

Furthermore, the SEM micrographs show irregular particle shapes that tend to grow with elongated and rounded edges. The shape of the particles can be considered due to the nanometric size of the precursors, particle agglomeration, and further fusion by the effect of the temperature.

The effect of neodymium on the microstructural characteristics is observed in the TEM micrographs, Fig. 7. Two samples sintered at 1050 °C have been analyzed with neodymium contents of $\times$ = 0.1 (S1-1050 °C) and $\times$ = 0.4 (S4-1050 °C). From these micrographs, it is observed that the neodymium stimulates the growth of particles. Although the sintering temperature also gives place to the growth of particles, some differences are observed in the particle growth

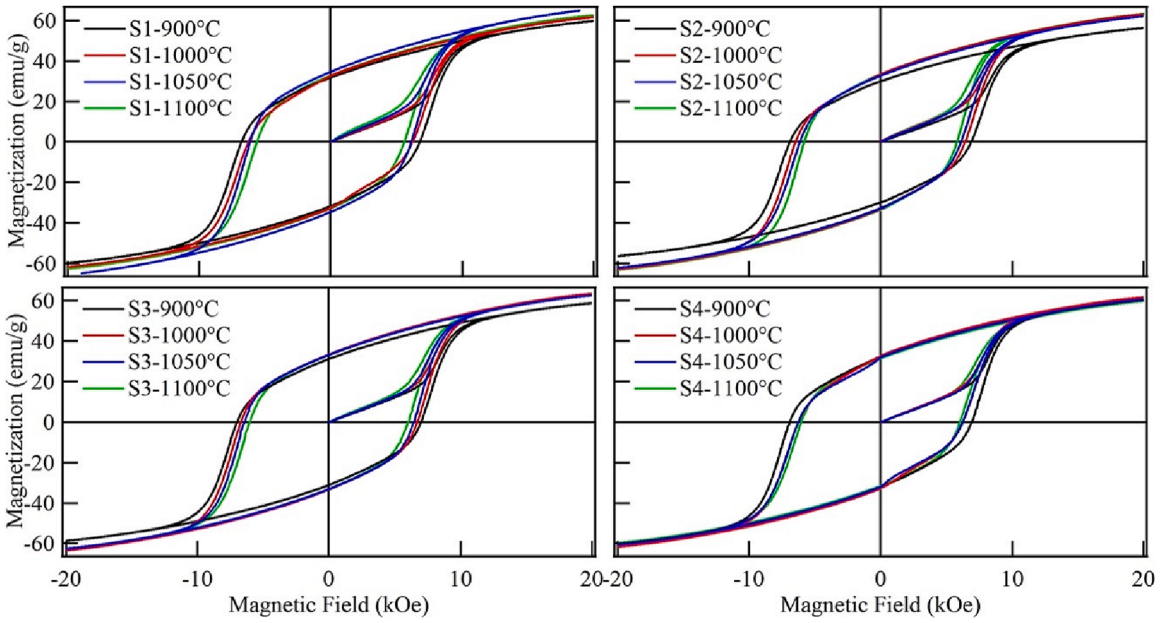

Fig. 8. Magnetization curves of the strontium hexaferrite at increasing neodymium content and sintering temperature from 900 °C to 1100 °C.

Table 2
Magnetic characterization of the hexaferrite varying the neodymium content and temperature.

Sample	M_r (emu/g)	M_s (emu/g)	M_r/M_s	H_c (kOe)	BH_{max} (kJ/m^3)
$SrFe_{12}O_{19}$	32.14	60.46	0.50	5.54	6.120
S1-900 °C	32.03	59.88	0.53	6.87	6.097
S1-1000 °C	32.64	61.78	0.52	6.26	8.185
S1-1050 °C	34.69	65.69	0.51	6.13	8.293
S1-1100 °C	33.60	62.65	0.51	5.54	7.474
S2-900 °C	32.06	60.30	0.53	6.88	6.334
S2-1000 °C	33.50	63.13	0.53	6.44	7.235
S2-1050 °C	32.85	62.13	0.53	6.13	7.444
S2-1100 °C	33.56	63.31	0.53	5.82	7.755
S3-900 °C	31.09	59.80	0.52	6.99	6.761
S3-1000 °C	33.32	63.57	0.52	6.70	7.724
S3-1050 °C	33.04	62.67	0.52	6.42	7.612
S3-1100 °C	33.02	62.88	0.52	6.02	7.581
S4-900 °C	32.06	60.40	0.53	6.92	7.164
S4-1000 °C	33.00	61.6	0.53	6.20	7.223
S4-1050 °C	31.89	60.73	0.52	6.26	6.296
S4-1100 °C	31.41	59.81	0.52	6.04	6.887

attributable to the sintering temperature and the amount of neodymium. Particles grown under the influence of temperature have a preferred orientation with rounded and irregular edges, evidencing the coalescence of smaller particles. On the other hand, particle growth caused by the neodymium influence shows uniform grain growth with sharp edges.

3.5. Magnetic properties

Fig. 8 shows the magnetization curves of the strontium hexaferrite with different neodymium contents and sintering temperatures. These curves show a clear variation in the coercive field (H_c), attributable to changes in the morphological characteristics of the hexaferrite particles. The magnetic properties are crucially dependent on both the shape and size of particles. As the morphological characterization showed, the particle size increased with increasing the calcination temperature. Therefore, a systematic reduction of the coercive field occurs with the increasing of crystal size, mainly in samples with × between 0.1 and 0.3. For the samples with × = 0.4, the coercive field is maintained after an initial reduction due to the high neodymium content. On the other hand, the observed changes in the saturation (M_s) and remanence (M_r) magnetizations are related to the incorporation of neodymium into the hexaferrite structure, although the presence of neodymium orthoferrite as a secondary phase also can affect the magnetic properties of the hexaferrite.

Table 2 shows the saturation magnetization, remanent magnetization, and coercive field taken from the hysteresis loops for all the analyzed samples. Also, the undoped strontium hexaferrite obtained by the sol–gel Pechini method at 1050 °C has been included as a reference. The squareness ratio (M_r/M_s) and the maximum energy product $(BH)_{max}$ were calculated and reported in Table 2. The squareness ratio is essentially a measure of the squareness of the hysteresis loop, and if $M_r/M_s \geq 0.5$, the material has a single-domain magnetic structure, but if $M_r/M_s < 0.5$, the material has a multi-domain magnetic structure [51]. The energy product $(BH)_{max}$ is a key figure of merit for a permanent magnet and is defined as the product of B and H in the second quadrant of the BH curve, where $B = H + 4\pi M$ [52]. The $(BH)_{max}$ relates to the magnet's ability to store magnetostatic energy in the free space [53].

Fig. 9 shows the magnetic properties of substituted strontium hexaferrites sintered at 900, 1000, 1050, and 1100 °C, depending on the neodymium content. The maximum coercive field was reached for the samples sintered at 900 °C. The coercive field showed a tendency to decrease in different manners with increasing the sintering temperature for samples with the same amount of neodymium. Here, the magnetization reversal may occur through a series of local processes depending on the particle size, but also from interparticle magnetic interactions, size distribution, surface disorder, inhomogeneities, and orientation of the magnetic axes [54]. These factors play a key role in maintaining a relatively high coercive field in those materials. Besides, it was proved that neodymium has a strong influence on the microstructure and magnetic properties of the hexaferrite. Thus, the sintering temperature and the neodymium content control the particle growth and other features which strongly affect the magnetization reversal. On the other hand, the saturation and remanent magnetizations show distinct behaviors probably influenced by factors such as structural changes promoted by the neodymium substitution and the magnetic interactions with the neodymium orthoferrite. Although these factors may be intertwined in complex ways, the maximum magnetization was achieved using lower Nd contents and sintering at 1050 °C, while the lowest magnetization values were obtained using high neodymium contents

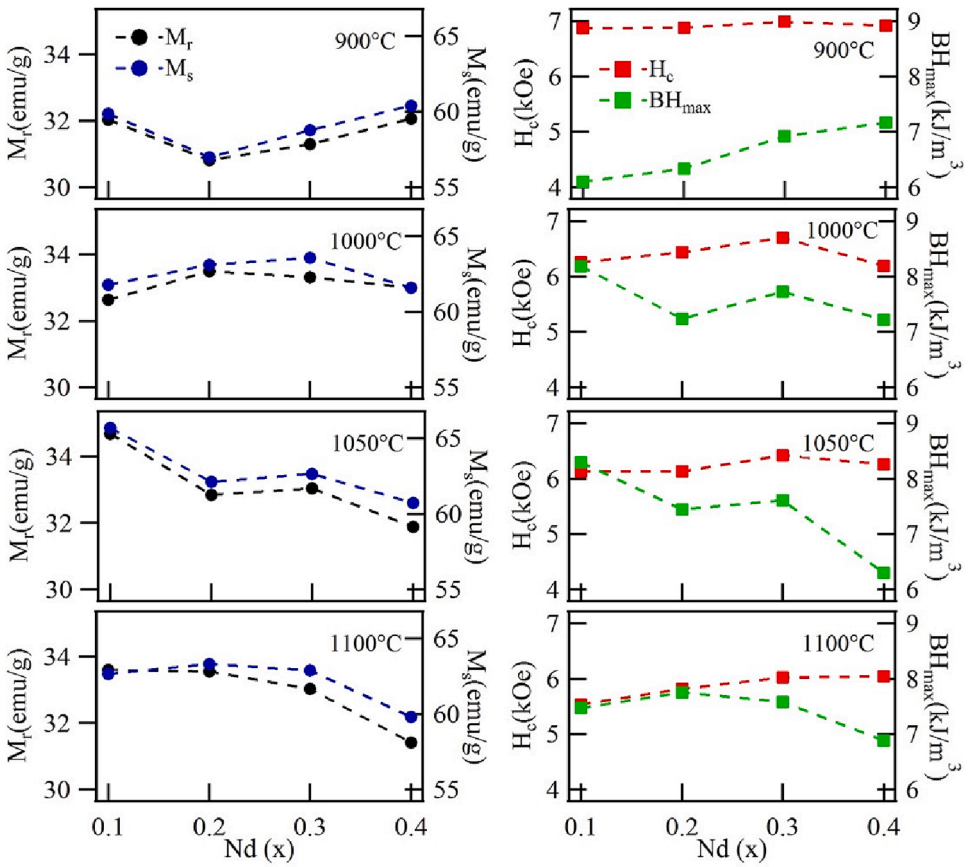

Fig. 9. Behavior of the magnetic parameters of the substituted hexaferrite calcined at temperatures between 900 °C and 1100 °C, presented as a function of the neodymium content.

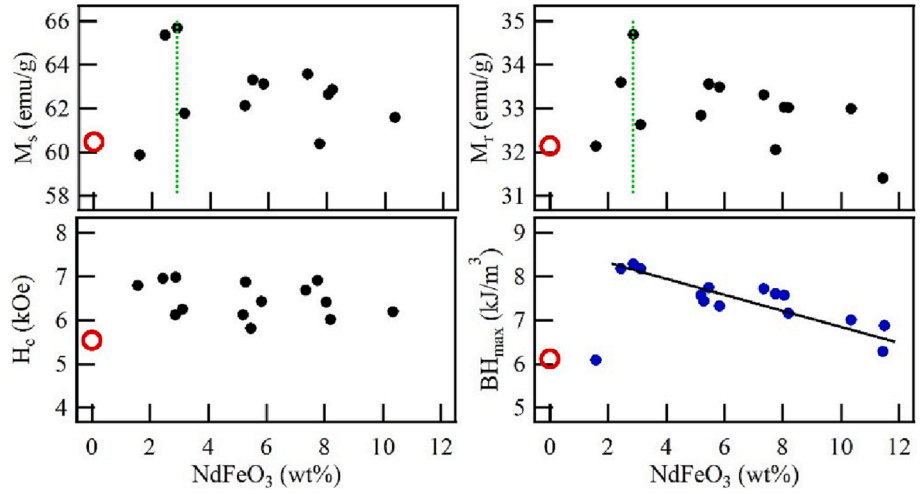

Fig. 10. Effect of the neodymium orthoferrite on the magnetic properties of the hexaferrite. (open circles correspond to the pure strontium hexaferrite).

and high sintering temperatures. The increase in magnetization M_r and M_s is mainly due to the better structural properties exhibited by the hexaferrite sintered at 1050 °C. However, these magnetizations decrease with increasing the amount of neodymium due to the formation of neodymium orthoferrite together with the hexaferrite. Here, high amounts of neodymium orthoferrite favor the demagnetizing-like interactions and reduce the magnetization values of the hexaferrite [55]. On the other hand, the maximum energy product correctly summarizes the behavior of the magnetic properties of the hexaferrite fabricated by the sol–gel Pechini method when varying the sintering temperature and the amount of neodymium.

Fig. 10 analyzes the effects caused by the presence of neodymium orthoferrite on the magnetic properties of hexaferrite. Although it has been established that small amounts of neodymium cations entering the crystalline structure can affect the magnetic and structural properties, also the presence of the neodymium orthoferrite appears to have a significant effect. The magnetic remanence, saturation, and maximum energy product significantly increment when a small amount of neodymium orthoferrite is formed with the hexaferrite. For example, the magnetic properties show maximum values when 2.85 %wt. of

neodymium orthoferrite is present with the hexaferrite. In this case, the remanence and saturation magnetizations show respective increments of 8.6 % and 7.9 % with respect to the unsubstituted strontium hexaferrite (red marks in Fig. 10), while the maximum energy product has an increment of 35 %. According to Vera-Serna et al. [56], the magnetic saturation of neodymium orthoferrite is 1.54 emu/g, the remanence is 0.26 emu/g and the coercive field is 0.37 kOe. These values are not significant to the values shown for the strontium hexaferrite. The enhanced magnetic properties of the hexaferrite are affected by complex aspects, including the structural and microstructural aspects, as well as the magnetization reversal processes. However, the magnetic interaction between hexaferrite and neodymium orthoferrite also strongly affects the magnetic properties of the hexaferrite. Two types of magnetic interactions can be presented between both magnetic phases: A type of magnetostatic interaction that emerges from the magnetic charges on grain boundaries and a type of exchange interaction that arises through grain surfaces [54]. The exchange interaction tends to align the magnetization in one direction and depends on the particle size. Small particle size improves exchange interactions. Meanwhile, the strength of the magnetostatic interaction mainly depends on the shape and arrangement of the particles.

4. Conclusions

The effects of changing the sintering temperature and neodymium content were systematically studied for the strontium hexaferrite obtained by the sol–gel Pechini method. Both temperature and neodymium content strongly affect the morphology, structure, and magnetic properties of the hexaferrite. This method only allowed a limited amount of neodymium to be incorporated into the hexaferrite structure, and the neodymium excess favored the formation of neodymium orthoferrite. Although it is difficult to identify the neodymium orthoferrite together with hexagonal ferrite due to the overlapping of diffraction peaks, the presence of neodymium orthoferrite significantly affected the magnetic properties of the hexaferrite. Results indicated that the magnetic interaction between both phases closely depends on the amount of neodymium orthoferrite. In particular, the magnetic properties reached their maximum values when the hexaferrite was accompanied by 2.85 % wt. of neodymium orthoferrite, which shows a 35% increment of the maximum energy product regarding the pure strontium hexaferrite.

CRediT authorship contribution statement

M.F. Ramírez-Ayala: Conceptualization, Formal analysis, Writing – original draft, Writing – review & editing. **A. Lobo Guerrero:** Conceptualization, Formal analysis, Writing – original draft, Writing – review & editing. **A.M. Herrera-González:** Resources, Methodology. **T.J. Pérez-Juache:** Methodology, Conceptualization, Supervision, Writing – original draft. **R. López-Juárez:** Investigation, Validation. **J.T. Elizalde-Galindo:** Investigation, Validation. **V.E. Salazar-Muñoz:** Resources, Methodology. **S.A. Palomares-Sánchez:** Resources, Methodology. **S.Y. Reyes-López:** Investigation, Validation.

Declaration of Competing Interest

The authors declare that they have no known competing financial interests or personal relationships that could have appeared to influence the work reported in this paper.

Data availability

Data will be made available on request.

Acknowledgments

M.F. Ramírez thanks to CONACyT (México) for her student grant 791363. R. López thanks to DGAPA-UNAM for financial support under project number IN113420. Thanks to Josué Romero (IIM-UNAM) and Neftalí Razo (ENES-Morelia) for TEM images and technical support, respectively.

References

[1] Z. Mosleh, P. Kameli, M. Ranjbar, H. Salamati, Effect of annealing temperature on structural and magnetic properties of $BaFe_{12}O_{19}$ hexaferrite nanoparticles, Ceram. Int. 40 (2014) 7279–7284, https://doi.org/10.1016/j.ceramint.2013.12.068.
[2] M.M.E. Barakat, D.E. Bakeer, A.H. Sakr, Structural, Magnetic Properties and Electron Paramagnetic Resonance for $BaFe_{12-x}Hg_xO_{19}$ Hexaferrite Nanoparticles Prepared by Co-Precipitation Method, J. Taibah Univ. Sci. 14 (2020) 640–652, https://doi.org/10.1080/16583655.2020.1761676.
[3] W. Onreabroy, K. Papato, G. Rujijanagul, K. Pengpat, T. Tunkasiri, Study of strontium ferrites substituted by lanthanum on the structural and magnetic properties, Ceram. Int. 38 (2012) 415–419, https://doi.org/10.1016/j.ceramint.2011.05.023.
[4] C. de Julián Fernández, C. Sangregorio, J. de la Figuera, B. Belec, D. Makovec, A. Quesada, Progress and prospects of hard hexaferrites for permanent magnet applications, J. Phys. D: Appl. Phys. 54 (2021) 1–30, https://doi.org/10.1088/1361-6463/abd272.
[5] M. Zahid, S. Siddique, R. Anum, F.F. Shakir, Y. Nawab, Z.A. Rehan, M-Type Barium Hexaferrite-Based Nanocomposites for EMI Shielding Application: A Review, J. Supercond. Nov. Magn. 34 (2021) 1019–1045, https://doi.org/10.1007/s10948-021-05859-1.
[6] J. Lee, Y.K. Hong, W. Lee, G.S. Abo, J. Park, N. Neveu, W.M. Seong, S.H. Park, W. K. Ahn, Soft M-type hexaferrite for very high frequency miniature antenna applications, J. Appl. Phys. 111 (2012) 1–3, https://doi.org/10.1063/1.3679468.
[7] M. Elansary, M. Belaiche, C. Ahmani Ferdi, E. Iffer, I. Bsoul, New nanosized Gd–Ho–Sm doped M-type strontium hexaferrite for water treatment application: experimental and theoretical investigations, RSC Adv. 10 (2020) 10–42, https://doi.org/10.1039/D0RA04722H.
[8] U.A. Rashid, P. Southern, J.A. Darr, S. Awan, S. Manzoor, Strontium hexaferrite ($SrFe_{12}O_{19}$) based composites for hyperthermia applications, J. Magn. Magn. Mater. 344 (2013) 134–139, https://doi.org/10.1016/j.jmmm.2013.05.048.
[9] M.I. Arshad, S. Nadeem, N. Amin, K. Mahmood, M. Ramzan, S. Arshad, A. Bibi, M. Ajaz-un-Nabi, Tailoring the Structural and Electrical Properties of Ba–Zn–Co M-Type Hexaferrites by Lanthanum Substitution for High-Resistivity Applications, J. Supercond. Nov. Magn. 34 (2020) 1807–1811, https://doi.org/10.1007/s10948-020-05750-5.
[10] G. Ferk, P. Krajnc, A. Hamler, A. Mertelj, F. Cebollada, M. Drofenik, D. Lisjak, Monolithic Magneto-Optical Nanocomposites of Barium Hexaferrite Platelets in PMMA, Sci. Rep. 5 (2015) 1–8, https://doi.org/10.1038/srep11395.
[11] A.V. Trukhanov, V.G. Kostishyn, L.V. Panina, V.V. Korovushkin, V.A. Turchenko, P. Thakur, A. Thakur, Y. Yang, D.A. Vinnik, E.S. Yakovenko, L.Y. Matzui, E. L. Trukhanova, S.V. Trukhanov, Control of electromagnetic properties in substituted M-type hexagonal ferrites, J. Alloys Compd. 754 (2018) 247–256, https://doi.org/10.1016/j.jallcom.2018.04.150.
[12] A.M. Adam, A. Elshafaie, E.M.M. Ibrahim, Structural and magnetic properties of Dy doped $SrFe_{12}O_{19}$ ferrites, Mat. Today Comm. 35 (2023), 105884, https://doi.org/10.1016/j.mtcomm.2023.105884.
[13] S.V. Trukhanov, A.V. Trukhanov, L.V. Panina, V.G. Kostishyn, V.A. Turchenko, E. L. Trukhanova, V. An, T.I. Trukhanov, V.M. Zubar, D.I. Ivanov, D.A. Tishkevich, S. A. Vinnik, D.S. Gudkova, M.G. Klygach, P. Vakhitov, A. Thakur, Y.Y. Thakur, Temperature evolution of the structure parameters and exchange interactions in $BaFe_{12-x}In_xO_{19}$, J. Magn. Magn. Mater. 466 (2018) 393–405, https://doi.org/10.1016/j.jmmm.2018.07.041.
[14] S.V. Trukhanov, A.V. Trukhanov, V.A. Turchenko, V. An, D.I. Trukhanov, E. L. Tishkevich, T.I. Trukhanova, D.V. Zubar, V.G. Karpinsky, L.V. Kostishyn, D. A. Panina, S.A. Vinnik, E.A. Gudkova, P. Trofimov, A. Thakur, Y.Y. Thakur, Magnetic and dipole moments in indium doped barium hexaferrites, J. Magn. Magn. Mater. 457 (2018) 83–96, https://doi.org/10.1016/j.jmmm.2018.02.078.
[15] D. Seifert, J. Töpfer, M. Stadelbauer, R. Grössinger, J.M. Le Breton, Rare-Earth-Substituted $Sr_{1-x}Ln_xFe_{12}O_{19}$ Hexagonal Ferrites, J. Am. Cer. Soc. 94 (2011) 2109–2118, https://doi.org/10.1111/j.1551-2916.2010.04363.x.
[16] K. Rana, P. Thakur, A. Thakur, M. Tomar, V. Gupta, J. Luc Mattei, P. Queffelec, Influence of samarium doping on magnetic and structural properties of M type Ba–Co hexaferrite, Ceram. Inter. 42 (2016) 8413–8418, https://doi.org/10.1016/j.ceramint.2016.02.058.
[17] K. Rana, P. Thakur, M. Tomar, V. Gupta, A. Thakur, Investigation of cobalt substituted M-type barium ferrite synthesized via co-precipitation method for radar absorbing material in Ku-band (12–18 GHz), Ceram. Inter. 44 (2018) 6370–6375, https://doi.org/10.1016/j.ceramint.2018.01.028.
[18] S. Goel, A. Garg, A. Tyagi, S. Tyagi, Influence of carbon black addition on the microwave absorption properties of neodymium-doped barium hexaferrite, J. Mater. Sci.: Mater. Electron. 34 (2023) 436, https://doi.org/10.1007/s10854-023-09880-z.
[19] A.V. Trukhanov, M.A. Darwish, L.V. Panina, A.T. Morchenko, V.G. Kostishyn, V. A. Turchenko, D.A. Vinnik, E.L. Trukhanova, K.A. Astapovich, A.L. Kozlovskiy, M. Zdorovets, S.V. Trukhanov, Features of crystal and magnetic structure of the $BaFe_{12-x}Ga_xO_{19}$ ($x \leq 2$) in the wide temperature range, J. Alloys Compd. 791 (2019) 522–529, https://doi.org/10.1016/j.jallcom.2019.03.314.

[20] B.H. Bhat, R. Samad, B. Want, Dielectric and impedance behavior of neodymium substituted strontium hexaferrite, Appl. Phys. A. 122 (2016) 1–11, https://doi.org/10.1007/s00339-016-0331-1.

[21] A. Hilczer, K. Pasińska, Dielectric response of $Sr_{0.95}Nd_{0.05}Fe_{12-x}Sc_xO_{19}$ hexaferrites nanoceramics as dependent on crystal and microstructure and ceramic heterogeneity, J. Alloys Compd. 893 (2022), 162303, https://doi.org/10.1016/j.jallcom.2021.162303.

[22] A. Garg, S. Goel, A.K. Dixit, M.K. Pandey, N. Kumari, S. Tyagi, Investigation on the effect of neodymium doping on the magnetic, dielectric and microwave absorption properties of strontium hexaferrite particles in X-band, Mater. Chem. Phys. 257 (2021) 1–9, https://doi.org/10.1016/j.matchemphys.2020.123771.

[23] T.J. Pérez, A.L. Guerrero, J.G. Cabal, M. Mirabal, S.A. Palomares, J.A. Matutes, Analysis of the structure and Mössbauer study of the neodymium substitution in the Sr-hexaferrite, Phys. B Condens. Matter. 503 (2016) 183–188, https://doi.org/10.1016/j.physb.2016.09.026.

[24] M. Effendi, E. Solihah, C. Kurniawan, W.T. Cahyanto, W. Widanarto, Transformation of Structure, Magnetic Properties and Microwave Absorption Capability in Nd-Doped Strontium Hexaferrite, Key Eng. Mater. 855 (2020) 255–260, https://doi.org/10.4028/www.scientific.net/KEM.855.255.

[25] Y.E. Gunanto, M.P. Izaak, H. Sitompul, W.A. Adi, Effect of Nd^{3+} substitution on the BH_{max} properties of barium-strontium hexaferrite permanent magnet, J. Phys.: Conf. Ser. 1825 (2021) 1–5, https://doi.org/10.1088/1742-6596/1825/1/012054.

[26] S. Goel, A. Garg, R.K. Gupta, A. Dubey, N.E. Prasad, S. Tyagi, Effect of neodymium doping on microwave absorption property of barium hexaferrite in X-band, Mater. Res. Express 7 (2020) 1–7, https://doi.org/10.1088/2053-1591/ab6544.

[27] J.R. Liu, R.Y. Hong, W.G. Feng, D. Badami, Y.Q. Wang, Large-scale production of strontium ferrite by molten-salt-assisted coprecipitation, Powder Technol. 262 (2014) 142–149, https://doi.org/10.1016/j.powtec.2014.04.076.

[28] A.V. Trukhanov, M.A. Almessiere, A. Baykal, S.V. Trukhanov, Y. Slimani, D. A. Vinnik, V.E. Zhivulin, A.Y. Starikov, D.S. Klygach, M.G. Vakhitov, T.I. Zubar, D. I. Tishkevich, E.L. Trukhanova, M. Zdorovets, Influence of the charge ordering and quantum effects in heterovalent substituted hexaferrites on their microwave characteristics, J. Alloys Compd. 788 (2019) 1193–1202, https://doi.org/10.1016/j.jallcom.2019.02.303.

[29] H. Sözeri, A. Baykal, B. Ünal, Low-temperature synthesis of single-domain Sr-hexaferrite particles by solid-state reaction route, Phys. Status Solidi A. 209 (2012) 1–12, https://doi.org/10.1002/pssa.201228023.

[30] K. Kim, K.W. Jeon, K.W. Moon, M.K. Kang, J. Kim, Effects of calcination conditions on magnetic properties in strontium ferrite synthesized by the molten salt method, IEEE Trans. Magn. 52 (2016) 1–4, https://doi.org/10.1109/TMAG.2016.2531119.

[31] R.L. Palomino, A.M. Bolarín Miró, F.N. Tenorio, F. Sánchez, C.A. Cortés, S. Ammar, Sonochemical assisted synthesis of $SrFe_{12}O_{19}$ nanoparticles, Ultrason. Sonochem. 29 (2016) 470–475, https://doi.org/10.1016/j.ultsonch.2015.10.023.

[32] M. Jean, V. Nachbaur, J. Bran, J.M. Le Breton, Synthesis and characterization of $SrFe_{12}O_{19}$ powder obtained by hydrothermal process, J. Alloys Compd. 496 (2010) 306–312, https://doi.org/10.1016/j.jallcom.2010.02.002.

[33] G.H. An, T.Y. Hwang, Y.H. Choa, K. Shin, Synthesis of size-controlled $SrFe_{12}O_{19}$ using modified spray pyrolysis–calcination method and their magnetic properties, J. Electron. Mater. 43 (2014) 3574–3581, https://doi.org/10.1007/s11664-014-3228-9.

[34] S.B. Galvão, A.C. Lima, S.N. De Medeiros, J.M. Soares, C.A. Paskocimas, The effect of the morphology on the magnetic properties of barium hexaferrite synthesized by Pechini method, Mater. Lett. 115 (2014) 38–41, https://doi.org/10.1016/j.matlet.2013.10.012.

[35] T. Kaur, S. Kumar, B.H. Bhat, A.K. Srivastava, Enhancement in physical properties of barium hexaferrite with substitution, J. Mater. Res. 30 (2015) 2753–2762, https://doi.org/10.1557/jmr.2015.244.

[36] J. Liu, X. Feng, S. Wu, P. Zhou, J. Huang, H. Li, T. Liang, High microwave absorption performance in Nd-substituted BaM/GO through sol-gel and high energy ball milling process, J. Alloys Compd. 892 (2022) 1–9, https://doi.org/10.1016/j.jallcom.2021.162207.

[37] A.E. Ramírez, N.J. Solarte, L.H. Singh, J.A.H. Coaquira, S. Gaona J. Investigation of the magnetic properties of $SrFe_{12}O_{19}$ synthesized by the Pechini and combustion methods. J. Magn. Magn. Mater. 438 (2017) 100-106. https://doi.org/10.1016/j.jmmm.2017.04.042.

[38] S.B. Galvão, A.C. Lima, S.N. de Medeiros, J.M. Soares, C.A. Paskocimas, The effect of the morphology on the magnetic properties of barium hexaferrite synthesized by Pechini method, Mater. Lett. 115 (2014) 38–41, https://doi.org/10.1016/j.matlet.2013.10.012.

[39] L. Lechevallier, J.M. Le Breton, A. Morel, P. Tenaud, Influence of the presence of Co on the rare earth solubility in M-type hexaferrite powders, J. Magn. Magn. Mater. 316 (2007) 109–111, https://doi.org/10.1016/j.jmmm.2007.02.042.

[40] L. Lechevallier, J.M. Le Breton, A. Morel, P. Tenaud, On the solubility of rare earths in M-type $SrFe_{12}O_{19}$ hexaferrite compounds, J. Phys.: Condens. Matter. 20 (17) (2008), 175203, https://doi.org/10.1088/0953-8984/20/17/175203.

[41] M.A. Urbano, S.A. Palomares, I. Betancourt, T.J. Pérez, F. Ruiz, Effect of temperature on the magnetic properties of strontium hexaferrite synthesized by the Pechini method, Appl. Phys. A. 125 (2019) 1–8, https://doi.org/10.1007/s00339-019-3004-z.

[42] L. Klein, M. Aparicio, A. Jitianu. Handbook of Sol-Gel science and technology: Processing, characterization and applications. Second ed., Kluwer, New York, 2018. https://doi.org/10.1007/978-3-319-32101-1.

[43] H. Putz, K. Brandenburg. Match-phase identification from powder diffraction–crystal impact software (V. 3.6.2.121). Putz, K. Brandenburg. Bonn, Germany. https://www.crystalimpact.de/match.

[44] L. Lutterotti, P. Scardi, Simultaneous structure and size–strain refinement by the Rietveld method, J. Appl. Crystallogr. 23 (1990) 246–252, https://doi.org/10.1107/S0021889890002382.

[45] S. Gražulis, A. Merkys, A. Vaitkus, D. Chateigner, L. Lutterotti, P. Moeck, M. Quiros, R.T. Downs, W. Kaminsky, A.L. Bail. Crystallography open database: History, development, and perspectives. O. Isayev, A. Trospsha, S. Curtarolo (Eds.). Materials Informatics: Methods, Tools and Applications. Wiley. Lithuania, 1-39. https://doi.org/10.1002/9783527802265.ch1.

[46] B.H. Toby, R factors in Rietveld analysis: How good is good enough? Powder Diffr. 21 (2006) 67–70, https://doi.org/10.1154/1.2179804.

[47] B. Want, B.H. Bhat, Magnetic and dielectric characteristics of Nd and Nd-Mg substituted strontium hexaferrite, Mod. Electron. Mater. 4 (2018) 21–29, https://doi.org/10.3897/j.moem.4.1.33273.

[48] S. Selvaraj, U. Gandhi, L.J. Berchmans, U. Mangalanathan, Effect of magnetic ion substitution on the structure and temperature-dependent magnetic properties of strontium hexaferrite, Mater Technol. 36 (2020) 36–45, https://doi.org/10.1080/10667857.2020.1723832.

[49] M.M. Hessien, N. El-Bagoury, M.H.H. Mahmoud, M. Alsawat, A.K. Alanazi, M. M. Rashad, Implementation of La^{3+} ion substituted M-type strontium hexaferrite powders for enhancement of magnetic properties, J. Magn. Magn. Mater. 498 (2020) 1–13, https://doi.org/10.1016/j.jmmm.2019.166187.

[50] N. Modaresi, R. Afzalzadeh, B. Aslibeiki, P. Kameli, A. Ghotbi, I. Orue, V. A. Chernenko, Magnetic properties of $Zn_xFe_{3-x}O_4$ nanoparticles: A competition between the effects of size and Zn doping level, J. Magn. Magn. Mater. 482 (2019) 206–218, https://doi.org/10.1016/j.jmmm.2019.03.060.

[51] I. Ali, M.U. Islam, M.S. Awan, M. Ahmad, Effects of Ga–Cr substitution on structural and magnetic properties of hexaferrite ($BaFe_{12}O_{19}$) synthesized by sol–gel auto-combustion route, J. Alloys Compd. 547 (2013) 118–125, https://doi.org/10.1016/j.jallcom.2012.08.122.

[52] L.M. Silva, R.B. da Silva, R.L. Silva, M.A. Morales, J.H. de Araújo, Improvement of $(BH)_{max}$ in Ba-hexaferrite doped with La and Co, Ceram. Int. 48 (16) (2022) 23224–23231.

[53] W. Zhang, B. Balasubramanian, P. Kharel, R. Pahari, S.R. Valloppilly, X. Li, L. Yue, R. Skomski, D.J. Sellmyer. High energy product of MnBi by field annealing and Sn alloying. APL Mater. 7 (2019) 1-5. https://doi.org/10.1063/1.5128659.

[54] P. Maltoni, S.A. Ivanov, G. Barucca, G. Varvaro, D. Peddis, R. Mathieu, Complex correlations between microstructure and magnetic behavior in $SrFe_{12}O_{19}$ hexaferrite nanoparticles, Sci. Rep. 11 (2021) 23307, https://doi.org/10.1038/s41598-021-02782-2.

[55] H. Fukunaga, H. Inoue, Effect of intergrain exchange interaction on magnetic properties in isotropic Nd-Fe-B magnets, Jpn. J. Appl. Phys. 31 (1992) 1347–1352, https://doi.org/10.1143/JJAP.31.1347.

[56] P. Vera Serna, C. García Campos, F. Sánchez de Jesús, A.M. Bolarín Miró, J. A. Juanico Lorán, J. Longwell, Mechanosynthesis, crystal structure and magnetic characterization of neodymium orthoferrite, Mater. Res. 19 (2016) 389–393, https://doi.org/10.1590/1980-5373-MR-2015-0214.